This is a repository copy of *Characterization of the Structural Environment of Dithionate Ions Associated with Their Role in the Crystal Habit Modification of Sodium Chlorate*.

White Rose Research Online URL for this paper:
http://eprints.whiterose.ac.uk/133237/

Version: Supplemental Material

SUPPLEMENTARY MATERIAL

Characterization of the Structural Environment of Dithionate Ions Associated with their Role in the Crystal Habit Modification of Sodium Chlorate

Zhipeng Lan,[1, #] Guilherme A. Calligaris,[2] Alan S. de Menezes,[2, ‡]
Adenilson O. dos Santos,[3] Xiaojun Lai,[1] Lisandro P. Cardoso[2] and Kevin J. Roberts[1]

Background information on the techniques of Extended X-Ray Absorption Fine Structure (EXAFS) and X-Ray Multiple Diffraction (XRMD) is provided here.

A1. EXTENDED X-RAY ABSORPTION FINE STRUCTURE

When material undergo electromagnetic (EM) waves absorption it normally experiences a smooth dependence of its linear absorption coefficient μ in respect of the incident wave energy E. However, it abruptly suffers discontinuities at some energies that corresponds to the X-rays range in the EM spectrum, and this phenomenon is known as Absorption Edges. A careful measure of both incident and transmitted intensity of X-rays which pass thru the material makes visible all the small features of a so call X-rays Absorption Fine Structure (XAFS), as seem in the Figure A1.1. At same time, XAFS can be summarized as two defined regions known as X-ray Absorption Near-Edge Structure (XANES) and Extended X-ray Absorption Fine Structure (EXAFS).
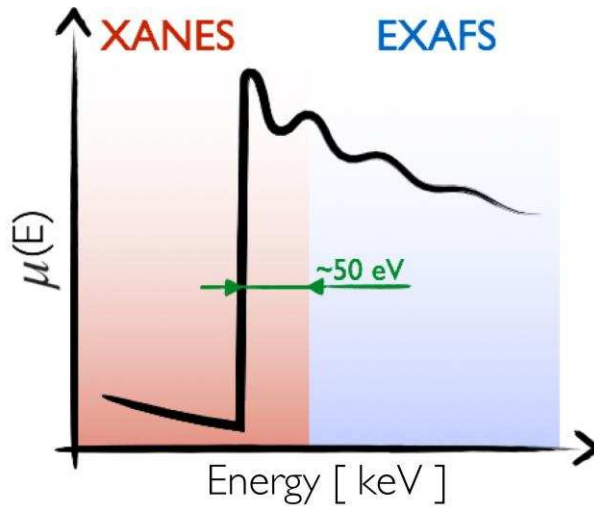
Figure A1.1 A general XAFS profile highlighting the two regions of XANES and EXAFS. EXAFS usually are defined after ~50 eV from the absorption edge and extends up to 1000 eV more, as long the oscillations persist.

The observed oscillations in a EXAFS measure arises from the interference of an outward-propagating spherical wave (described by an ejected photoelectron) centered in the absorbing element (absorbing atom) with the backscattered wave from a neighbor atom (scattering atom). In Quantum Mechanics this process is usually referred as the interference in the final-state wave functions. The energy of the photoelectron depends on the difference of the incident EM wave energy E and the absorption energy E_0, and same do its wavelength that is described as

$$\lambda(E) = \frac{h}{\sqrt{2m(E - E_0)}} \quad ,$$

(A1.1)

where h is the Planck's constant and m the electron mass. The related wave number k can be written as

$$k = \frac{2\pi}{\lambda} \quad ,$$

(A1.2)

and therefore has unit of Å^{-1}.

Because of such interference, the linear absorption coefficient μ of an atom from the studied material, i.e. the experimental μ, can be described in terms of k and the linear absorption coefficient μ_0 of a free atom of the same element as

$$\mu = \mu_0[1 - \chi(k)] \quad , \tag{A1.3}$$

where χ(k) describes the EXAFS oscillation. By assuming only dipole interactions between the absorbing element and the scattered wave, neglecting incident beam polarization and single scattering of a ~50 eV (or higher) photoelectron, the expression of the EXAFS signal is given by[1]

$$\chi(k) = \sum_j A_j(k)e^{-\beta_j(k)} \sin(2kR_j + \Phi_j(k)) \quad , \tag{A1.4}$$

$$A_j(k) = \frac{N_j}{kR_j^2} f_j(k)S_0^2 \quad , \tag{A1.5}$$

$$e^{-\beta_j(k)} = \exp\left[\frac{-2R_j}{\lambda_e}\right] \exp\left[-2k^2\sigma_j^2\right] \quad , \tag{A1.6}$$

where the term $2kR_j$ is the sine function argument that results from the phase of a photoelectron which described the path of leaving the absorbing atom and return as backscattered from a neighboring atom positioned at Rj. The other phase shift Φ_j(k) describes the phase-shift of the absorber atom and the phase-shift of the jth backscattering atom. A_j(k) is the amplitude term defined by N_j atoms of each shell and the scattering complex function magnitude f_j(k). S_0^2 is an amplitude reduction factor arising from many body effects. Both Φ_j(k) and f_j(k) depends on the atomic number Z_j. The exponential damping factor (A1.6) corresponds to the finite lifetime of the final state (~femtoseconds)

which is related to the photoelectron mean free path λ_e. The second exponential decay is defined in terms of the likewise a Debye-Waller parameter, σ_j^2 and describes the thermal contribution that disturbs the absorbing and scattering atoms original positions.

Original data is normalized based on the first peak after the absorption edge, which in turn is evaluated by a step function. Post-edge region background is described by a spline line and its difference between the experimental curve defines the $\chi(k)$. The obtained result is plotted in the k space and modern programs based on FEFF (stands for $f_{eff}(k,r)$, an effective scattering amplitude), such as Demeter suite[2], is used to fit $\chi(k)$. Fitting data before doing a Fourier transform (FT) helps avoid Fourier filtering issues. Only then original data and best fit are transformed to the real space "r" to a radial structure function. Gaussian distribution (based on σ parameter) describes the radial position of the neighboring atoms from the absorbing element.

XAFS is being widely applied in determining the chemical state and local atomic environment of a specific atom by tuning the incident X-ray energy near to its absorption edges. In the study of chemical bonds in different sulphur compounds is possible to highlight the work by Sekiyama et. al.[3]. The polarization from synchrotron sources can also provide the necessary tool to the determine the orientation of chemical bonds, as demonstrated by Tyson et al. by verify the electronic structure and molecular orientation of $S_2O_3^{2-}$ and $S_2O_6^{2-}$ in ionic crystals[4] and Yano et al. by determining the orientation of Mn-O and Mn-N bonds in complex compounds[5].

A2. X-RAY MULTIPLE DIFFRACTION

The multiple diffraction phenomenon occurs when an incident beam simultaneously satisfies Bragg's law for more than one set of lattice planes within the crystal. X-Ray Multiple Diffraction (XRMD) is generated by aligning the primary planes ($h_Pk_Pl_P$), and so the

primary reciprocal lattice vector H_P, to diffract the incident beam S_O into the primary beam S_P by adjusting the angle ω. Then, by rotating the azimuthal angle (ϕ) the sample revolute around H_P while monitoring the intensity of the primary diffracted beam $I_{primary}$. During the ϕ axis rotation, at certain specific angular positions, other crystallographic planes called secondary planes ($h_S k_S l_S$) (related to the secondary reciprocal lattice vector H_S) will also satisfy diffraction conditions and generates the secondary beam S_S in a distinct direction from that of the S_P beam. The S_S beam will be reflected back into the same direction as that of the S_P by interaction with another coupling plane ($h_C k_C l_C$), coupling beam S_C, and scattering vector H_C. An overview of this process in shown in Figure A2.1(a) using the Ewald sphere representation for diffraction conditions.

Based on this, secondary reflections can touch the Ewald sphere two times for each full revolution of the ϕ axis, from outside to inside (angle ϕ_{o-i}) and vice-versa (angle ϕ_{i-o}) with respect to a reference angle ϕ_0. The interaction between primary and secondary beams appears in the measure of $I_{primary}$ versus ϕ, which is referred to as a Renninger Scan[6] (RS), as positive (Umweganregung) and negative (Aufhellung) peaks. Those peaks can appear in pairs describing a symmetry mirror with respect to the chosen primary vector and the angular distance 2β between ϕ_{o-i} and ϕ_{i-o}. Figure A2.1(b) describes this angles. Such peaks represent energy transfer from the secondary beam into the path of the primary diffraction (positive peak), or vice versa (negative peak), with the symmetry mirror being established by the ϕ rotation when the secondary reciprocal lattice points enter and leave the Ewald sphere. Therefore, in a RS one can clearly observe the position and intensity distributions of these symmetry mirrors and these features are essential for most of the applications using the RS XRMD technique. The overall shape of a RS diffraction peak profile as a function of ϕ also provides a good indication on regards crystallographic symmetry and perfection. In this, splitting of some peaks can provide evidence for symmetry reduction,

e.g. due to (say) a tetragonal distortion in epitaxial layers[7] whilst an increase in peak width can indicate a reduction in crystal quality.[8] When a peak in the RS represents an interaction of the incident, primary and one secondary beam, it shows up as a three-beam peak (or three-beam case). One can also have two or more secondary beams interacting simultaneously.

Figure A2.1(c) represents S_0, S_P, S_S, and S_C in the real space together with the sample and the related planes in a generic XRMD case. Particularly, a special three-beam XRMD case, called Bragg-Surface Diffraction (BSD),[9] appears when the secondary beam propagates parallel to the crystal surface under an extremely asymmetric diffraction geometry. The BSD beams are of particular interest in this work that they carry information regarding the crystallography of the sample surface region (and interfaces when they occur) which is most useful for studying the structural impact of impurity incorporation at the growing crystal surface.[10, 11] The XRMD technique's ability to characterize lattice strain fields at the interfaces has been applied e.g. to epilayer/substrate in semiconductor systems revealing a depth penetration resolution of about 2 Å and with enough sensitivity to detect lattice distortions in the range of 72 Å around the epilayer/substrate interface.[12]
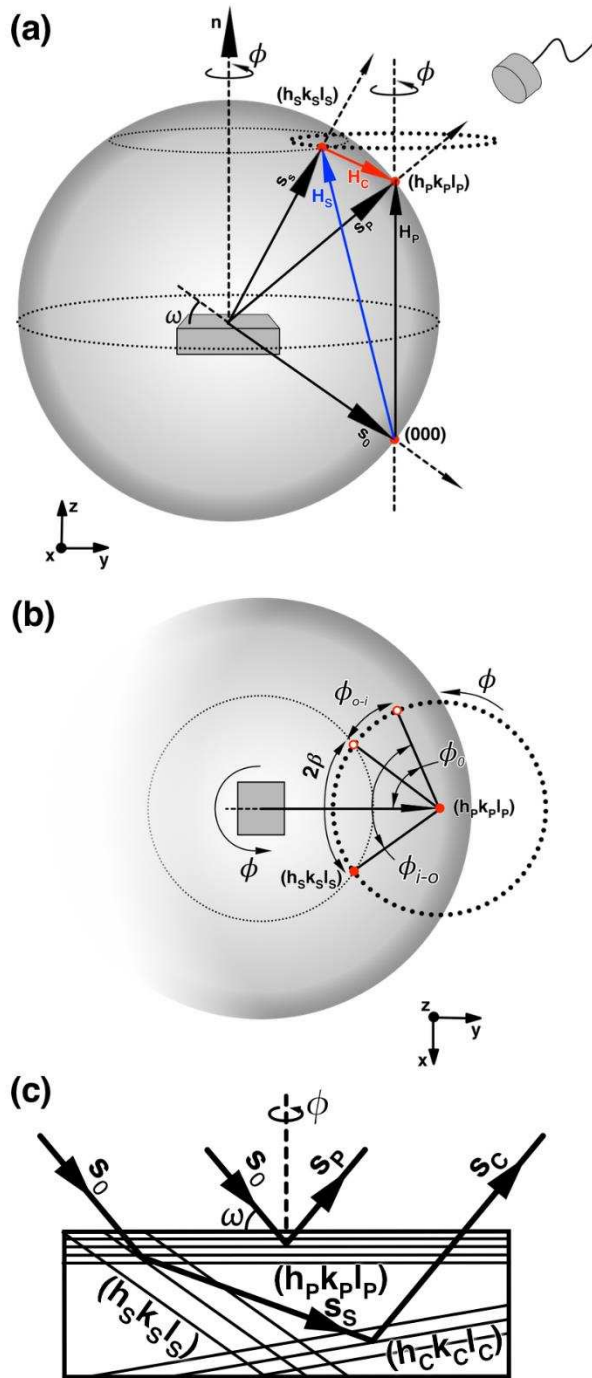
Figure A2.1 (a) XRMD phenomena represented using the Ewald sphere, showing S_0: (000), S_P: $(h_P k_P l_P)$ and S_S: $(h_S k_S l_S)$ in a general 3-beam case. Scattering vectors H_P, H_S and H_C are also shown. **(b)** A top view of the ϕ axis rotation showing the 2β, ϕ_{o-i}, ϕ_{i-o} angles between the entrance and exit of the $(h_S k_S l_S)$ reciprocal lattice point. **(c)** A side view in the real space of the XRMD process.

Also, in the XRMD technique, complementary and additional information regarding crystalline quality can be obtained from the detailed analysis of the exact multiple diffraction condition, through the $\omega{:}\phi$ mapping[8]. This method involves coupled scans of ω, the incident angle, with respect to the diffraction lattice planes and ϕ, the azimuthal rotation angle with respect to the primary reflection vector. In the mapping process, ω is scanned within a certain range at discrete ϕ positions as identified by tailoring an exact $\omega{:}\phi$ angular for an observed multiple-beam diffraction position. Therefore, this mapping produces a three-dimensional plot of the primary intensity versus ω and ϕ in a coupled way that the crystalline perfection can be evaluate by taking the full width half maximum (FWHM) values from ω and ϕ scans. When a BSD case is analyzed, the mapping can be related to the mosaic spread along the perpendicular and in-plane crystallographic directions, respectively.[13]

The indexation of a XRMD case is shown as $(000)(h_P k_P l_P)(h_{s_1} k_{s_1} l_{s_1})(h_{s_2} k_{s_2} l_{s_2})\ldots(h_{s_n} k_{s_n} l_{s_n})$. So, a general 3-beam case has the incident (000), one primary and one secondary beam. The coupling plane can be obtained by the relation

$$
\begin{aligned}
h_P &= h_S + h_C & , \\
k_P &= k_S + k_C & \text{and} \\
l_P &= l_S + l_C & .
\end{aligned}
\tag{A2.1}
$$

The utility of XRMD in material science has been previously demonstrated in terms of investigating the subtle changes in the crystal lattices under the application of an external electric field, allowing in turn the determination of piezoelectric coefficients of single crystals.[14, 15] This technique was also used to study the impurity incorporation mechanism, crystal perfection and habit modification of Mn^{3+} ion doped KDP crystals.[10, 11, 16] In ion-implanted semiconductors, XRMD has provided a method to accurately discriminate

between mosaic and nearly perfect crystals and the technique has been demonstrated to be sensitive enough to analyze lattice strain perpendicular and parallel to the crystal surfaces.[8, 17]

References

(1) Bunker, G., Introduction to XAFS : a practical guide to X-ray absorption fine structure spectroscopy. Cambridge University Press: Cambridge; New York, 2010.

(2) Ravel, B.; Newville, M., ATHENA, ARTEMIS, HEPHAESTUS: data analysis for X-ray absorption spectroscopy using IFEFFIT. Journal of Synchrotron Radiation **2005,** 12, (4), 537-541.

(3) Sekiyama, H.; Kosugi, N.; Kuroda, H.; Ohta, T., Sulfur K-edge absorption spectra of Na2SO4, Na2SO3, Na2S2O3, and Na2S2Ox (x=5-8). Bull. Chem. Soc. Jpn. **1986,** 59, (2), 575-579.

(4) Tyson, T. A.; Roe, A. L.; Frank, P.; Hodgson, K. O.; Hedman, B., Polarized experimental and theoretical \textit{K} -edge x-ray absorption studies of ${\mathrm{SO}}_{4}^{2\mathrm{-}}$, ${\mathrm{ClO}}_{3}^{\mathrm{-}}$, ${\mathrm{S}}_{2}$${\mathrm{O}}_{3}^{2\mathrm{-}}$, and ${\mathrm{S}}_{2}$${\mathrm{O}}_{6}^{2\mathrm{-}}$. Physical Review B **1989,** 39, (10), 6305-6315.

(5) Yano, J.; Robblee, J.; Pushkar, Y.; Marcus, M. A.; Bendix, J.; Workman, J. M.; Collins, T. J.; Solomon, E. I.; DeBeer George, S.; Yachandra, V. K., Polarized X-ray Absorption Spectroscopy of Single-Crystal Mn(V) Complexes Relevant to the Oxygen-Evolving Complex of Photosystem II. Journal of the American Chemical Society **2007,** 129, (43), 12989-13000.

(6) Renninger, M., „Umweganregung", eine bisher unbeachtete Wechselwirkungserscheinung bei Raumgitterinterferenzen. Zeitschrift für Physik A Hadrons and Nuclei **1937,** 106, (3), 141-176.

(7) de Menezes, A. S.; dos Santos, A. O.; Almeida, J. M. A.; Bortoleto, J. R. R.; Cotta, M. A.; Morelhão, S. L.; Cardoso, L. P., Direct Observation of Tetragonal Distortion in Epitaxial Structures through Secondary Peak Split in a Synchrotron Radiation Renninger Scan. Crystal Growth & Design **2010,** 10, (8), 3436-3441.

(8) Morelhão, S. L.; Cardoso, L. P., X-ray Multiple Diffraction Phenomenon in the Evaluation of Semiconductor Crystalline Perfection. Journal of Applied Crystallography **1996,** 29, (4), 446-456.

(9) Morelhão, S. L.; Cardoso, L. P., Structural properties of heteroepitaxial systems using hybrid multiple diffraction in Renninger scans. Journal of Applied Physics **1993,** 73, (9), 4218-4226.

(10) Lai, X.; Roberts, K. J.; Avanci, L. H.; Cardoso, L. P.; Sasaki, J. M., Habit modification of nearly perfect single crystals of potassium dihydrogen phosphate (KDP) by trivalent manganese ions studied using synchrotron radiation X-ray multiple diffraction in Renninger scanning mode. Journal of Applied Crystallography **2003,** 36, 1230-1235.

(11) Remédios, C. M. R.; dos Santos, A. O.; Lai, X.; Roberts, K. J.; Moreira, S. G. C.; Miranda, M. A. R.; de Menezes, A. S.; Rouxinol, F. P.; Cardoso, L. P., Experimental Evidence for the Influence of Mn^{3+} Concentration on the Impurity Incorporation and Habit Modification Mechanism of Potassium Dihydrogen Phosphate. Crystal Growth & Design **2010,** 10, (3), 1053-1058.

(12) Sun, W. C.; Chang, H. C.; Wu, B. K.; Chen, Y. R.; Chu, C. H.; Chang, S. L.; Hong, M.; Tang, M. T.; Stetsko, Y. P., Measuring interface strains at the atomic resolution in depth using x-ray Bragg-surface diffraction. Applied Physics Letters **2006,** 89, (9), 091915.

(13) Avanci, L. H.; Hayashi, M. A.; Cardoso, L. P.; Morelhao, S. L.; Riesz, F.; Rakennus, K.; Hakkarainen, T., Mapping of Bragg-surface diffraction of InP/GaAs(100) structure. Journal of Crystal Growth **1998,** 188, (1-4), 220-224.

(14) Avanci, L. H.; Cardoso, L. P.; Girdwood, S. E.; Pugh, D.; Sherwood, J. N.; Roberts, K. J., Piezoelectric coefficients of mNA organic nonlinear optical material using synchrotron X-ray multiple diffraction. Physical Review Letters **1998,** 81, (24), 5426-5429.

(15) Avanci, L. H.; Cardoso, L. P.; Sasaki, J. M.; Girdwood, S. E.; Roberts, K. J.; Pugh, D.; Sherwood, J. N., Synchrotron-radiation x-ray multiple diffraction applied to the study of electric-field-induced strain in an organic nonlinear optical material. Physical Review B **2000,** 61, (10), 6507-6514.

(16) Remédios, C. M. R.; Paraguassu, W.; Freire, P. T. C.; Mendes, J.; Sasaki, J. M.; Melo, F. E. A., Temperature studies of KH2PO4 : Mn crystals using x-ray diffraction and polarized Raman scattering. Physical Review B **2005,** 72, (1), 014121.

(17) Hayashi, M. A.; Morelhão, S. L.; Avanci, L. H.; Cardoso, L. P.; Sasaki, J. M.; Kretly, L. C.; Chang, S. L., Sensitivity of Bragg surface diffraction to analyze ion-implanted semiconductors. Applied Physics Letters **1997,** 71, (18), 2614-2616.